Aalborg Universitet

AALBORG UNIVERSITY

DENMARK

Experimental Validation of the Reverberation Effect in Room Electromagnetics

Steinböck, Gerhard; Pedersen, Troels; Fleury, Bernard Henri; Wang, Wei; Raulefs, Ronald

Link to publication from Aalborg University

Experimental Validation of the Reverberation Effect in Room Electromagnetics

Gerhard Steinböck, Troels Pedersen, Bernard Henri Fleury, Wei Wang and Ronald Raulefs

Abstract—The delay power spectrum is widely used in both communication and localization communities for characterizing the temporal dispersion of the radio channel. Experimental investigations of in-room radio environments indicate that the delay power spectrum exhibits an exponentially decaying tail. This tail can be characterized with Sabine's or Eyring's reverberation models, which were initially developed in acoustics. So far, these models were only fitted to data collected from radio measurements, but no thorough validation of their prediction ability in electromagnetics has been performed yet. This paper provides a contribution to fill this gap.

We follow Sabine's original experimental approach, which consists in comparing model predictions to experimental observations in a room, while varying its mean absorption coefficient and total room surface. We find that Eyring's model provides a more accurate prediction of the parameters characterizing the decaying tail, like the reverberation time, than Sabine's model.

We further use the reverberation models to predict the parameters of a recently proposed model of a distance-dependent delay power spectrum. This model enables us to predict the path loss, mean delay and rms delay spread versus transmitter-receiver distance. We observe good agreement between predictions and experimental results.

I. INTRODUCTION

Models describing the time dispersion of the radio channel are important tools to the engineering of wireless communication [1] and localization systems [2]. A standard approach used in the community to characterize time dispersion is by means of the delay power spectrum (average delay-power profile). Reference [1] gives a survey of the many models of the radio channel involving the delay power spectrum that have been proposed.

A common assumption for the delay power spectrum is the exponentially decaying tail [1]. One important parameter of the tail is the decay rate. The decay rate may be obtained empirically as in [3] or from models that express the decay rate as a function of other parameters characterizing the propagation environment by means of certain assumptions on the prevailing propagation conditions. Sabine's [4] and Eyring's [5] reverberation models are two examples of such models,

which have found a wide application in acoustics. These models describe the decay rate – also known as reverberation time – as a function of the average absorption coefficient, the volume, and the surface area specific to the considered room. This simplicity has motivated recent applications of Sabine's and Eyring's models to electromagnetics in [6]–[10].

Despite the striking similarity of delay power spectra observed in acoustics and electromagnetics, the mechanisms governing acoustic and electromagnetic propagation exhibit specific differences. As a result, the validity of Sabine's and Eyring's models in electromagnetics is not guaranteed to hold a priori. For instance, one fundamental assumption made in acoustical reverberation theory is that the attenuation through wall transmission is so high that in most cases it can be safely assumed that energy leaving the room does not reenter. That is, reverberation is confined to the room and the energy lost due to transmission is included in the absorption coefficient [4], [11]. In electromagnetics, similar assumptions are made for rooms with highly conductive walls, such as reverberation chambers [10], [12]. In typical indoor environments in which wireless systems are deployed, however, radio waves propagate easily through indoor wall materials, such as plasterboards, light bricks, or wood panels. Thus, it is unclear whether the fundamental assumption that reverberation is confined to a room is valid in these environments.

Several publications report estimates of the reverberation time and the average absorption coefficient in electromagnetics [6]–[10]. Common to these contributions is the experimental approach: these estimates were computed from measurements collected in several rooms with different characteristics (in volume, surface area, and absorption coefficient). This makes it rather impossible to come with any conclusive interpretation of the cause of observed differences between estimates obtained for different rooms. To the best of our knowledge, no systematic evaluation of the electromagnetic reverberation phenomenon has appeared in the literature for typical indoor environments.

In this contribution we validate and compare Sabine's [4], [11] and Eyring's [5], [11] reverberation models in typical indoor radio environments. Inspired by Sabine's original work [4], we carry out an experiment in which we change in a controlled systematic manner the average absorption coefficient and total surface area of a room and observe the effect on the reverberation time. This approach enables us to test the models' prediction capability by comparing predicted values to experimental results. Specifically, with this systematic approach i) we investigate if the reverberation is confined within a single room, ii) we compare the prediction accuracy of

Sabine's and Eyring's models and iii) we evaluate their validity in room electromagnetics. Furthermore, we use the two models to predict values of the reverberation parameters in an adjacent room. By inserting the predicted values in the model of the delay power spectrum model presented in [3] we predict the path gain (inverse of path loss), the mean delay, and the root mean square (rms) delay spread versus distance in the adjacent room. These predictions agree well with estimates obtained from measurements. Our systematic investigation finds both Sabine's and Eyring's models valid for room electromagnetics, but Eyring's model provides better prediction.

II. REVERBERATION MODELS

In the following we review Sabine's and Eyring's reverberation models in the context of radio channels and show how these models are related to the delay power spectrum model proposed in [3].

The delay power spectrum is defined as

$$G(d,\tau) = \mathrm{E}[|h(d,\tau)|^2], \tag{1}$$

where $h(d,\tau)$ denotes the channel impulse response with transmitter-receiver distance d. The expectation operator $\mathrm{E}[\,\cdot\,]$ represents the mathematical abstraction of an averaging procedure to suppress variations due to small and large scale fading. As shown in [3] and sketched in Fig. 1, $G(d,\tau)$ can be modeled as the sum of a primary component and a reverberant component:

$$G(d,\tau) = G_{\mathrm{pri}}(d,\tau) + G_{\mathrm{rev}}(d,\tau), \tag{2}$$

$$G_{\mathrm{pri}}(d,\tau) = G_0 \left(\frac{d_0}{d}\right)^n \delta\left(\tau - \frac{d}{c}\right) \tag{3}$$

$$G_{\mathrm{rev}}(d,\tau) = G_{0,\mathrm{rev}}\, e^{-\tau/T}\, u(\tau - \tfrac{d}{c}) \tag{4}$$

with $\delta(\,\cdot\,)$ denoting the Dirac delta function and $u(\,\cdot\,)$ being the unit step function. The primary component $G_{\mathrm{pri}}(d,\tau)$ represents the early part of the delay power spectrum. It results from the direct propagation and possibly first-order reflections. The parameters of the primary component are the reference path gain G_0 at reference distance d_0, the path gain exponent n, the speed of light c and the distance d between the transmitter and the receiver. The reverberant component $G_{\mathrm{rev}}(d,\tau)$ results from the multitude of higher order reflections in the room. As observed in measured delay power spectra, it decays exponentially with rate T, referred to as the reverberation time, onset d/c, and the reverberation reference gain $G_{0,\mathrm{rev}}$.

The received power $P_{\mathrm{R}}(t,d)$ originating from the reverberant component reads

$$P_{\mathrm{R}}(t,d) = \int P_{\mathrm{I}}(t-\tau)\, G_{\mathrm{rev}}(d,\tau)\, \mathrm{d}\tau, \tag{5}$$

where $P_{\mathrm{I}}(t)$ is the "input power" radiated by the transmitter. (Antennas losses are accounted for in $G_{\mathrm{rev}}(d,\tau)$.) The main concern of this work is to predict the parameters $G_{0,\mathrm{rev}}$ and T which describe $G_{\mathrm{rev}}(d,\tau)$. Thus, in the following we focus on models for $G_{\mathrm{rev}}(d,\tau)$.
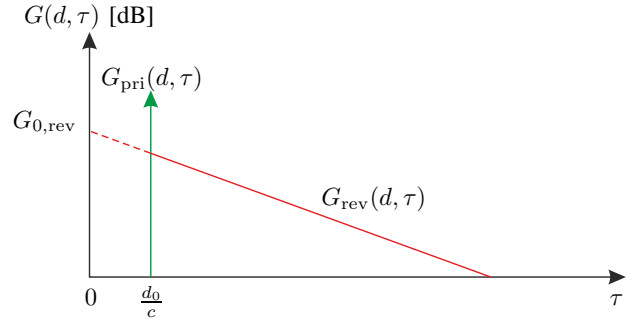

Fig. 1. The delay power spectrum and its relevant components and parameters according to the model in [3].

The average power $P_{\mathrm{R}}(t)$ received at an antenna immersed in an isotropic diffuse field is related to the energy density $W(t)$ in the room as [8], [10]

$$P_{\mathrm{R}}(t) = c\, A_{\mathrm{R}}\, W(t). \tag{6}$$

The proportionality constant A_{R} accounts for losses in the receive and transmit antennas. The energy density $W(t)$ has been characterized in [6]–[9], [13], [14] via reverberation models for room electromagnetics transposed from room acoustics. The isotropic diffuse field makes the impact of the directivity of the antennas negligible. In the following investigations, we assume no a priori information about the antenna characteristics. Therefore, we limit our investigations to relative changes in $P_{\mathrm{R}}(t)$ caused by controlled changes in the environment.

Similar models of the electromagnetic field prevailing in reverberation chambers exist [10]. These chambers have highly conductive walls and usually contain a mode stirrer. The propagation conditions prevailing in these chambers are obviously very different from those occurring in the type of rooms that we consider in this contribution: offices, meeting rooms, etc. It is therefore relevant to investigate if the reverberation models are applicable in rooms with non-ideal reverberation conditions. Reverberation models have been already applied to such rooms [6]–[9], [13], [14], however, their validity was not verified.

A. Sabine's Model

The seminal model for room acoustics by Sabine [4] is considered for in-room radio channels in [8], [9], [14], [15]. Sabine's model relies on the assumption of a diffuse field contained in a room. This assumption yields an expression for $W(t)$ by considering a closed room with volume V and surface area S, a single source inside the room and no contribution from outside the room. Upon wall interactions some power $(1-\bar{a})P_{\mathrm{I}}$ remains in the room while the rest $\bar{a}P_{\mathrm{I}}$ vanishes via absorption or transmission. The average absorption coefficient is defined as

$$\bar{a} = \frac{\sum_i S_i a_i}{S}, \tag{7}$$

where S_i denotes the surface area i with absorption coefficient a_i and $S = \sum_i S_i$ is the total surface area. It is shown in [8],

[11], [15] that the power balance of an isotropic diffuse field is described by the identity

$$\underbrace{P_\mathrm{I}(t)}_{\text{Input Power}} = \underbrace{V\frac{\mathrm{d}W(t)}{\mathrm{d}t}}_{\text{Reverberant Power}} + \underbrace{\frac{\bar{a}\,S\,c}{4}W(t)}_{\text{Absorbed Power}} . \tag{8}$$

The general solution of this first order differential equation is the convolutional integral

$$W(d,t) = \int_{-\infty}^{\infty} P_\mathrm{I}(t-\tau)\frac{1}{V}\exp\left(-\frac{\tau}{T_\mathrm{Sab}}\right)u(\tau-\tfrac{d}{c})\,\mathrm{d}\tau \tag{9}$$

with the reverberation time

$$T_\mathrm{Sab} = \frac{4\,V}{\bar{a}\,S\,c}. \tag{10}$$

Inserting (9) into (8) and comparing this to (5) and (6) we obtain an expression for the reverberant component as

$$G_\mathrm{rev,Sab}(d,\tau) = c\,A_\mathrm{R}\frac{1}{V}\exp\left(-\frac{\tau}{T_\mathrm{Sab}}\right)u(\tau-\tfrac{d}{c}). \tag{11}$$

B. Eyring's Model

As pointed out by Eyring [5], Sabine's model is inappropriate for rooms with high average absorption coefficients. Indeed by $\bar{a} = 1$ no reverberation occurs, but Sabine's model (10) still provides a positive value for the reverberation time. This observation led Eyring to propose a model suitable for large absorption coefficients [5].

Eyring's model is based on the mirror source theory [16] and does not rely on the assumption of the existence of a diffuse field [5]. Assuming specular only reflections, the propagation mechanisms between the transmitter and the receiver can be modeled geometrically via "virtual" mirror sources. For cavities this leads to infinitely many such mirror sources representing multiple wall reflections [5]. Upon incoherent addition of the signals originating from the mirror sources the total received signal reads

$$P_\mathrm{R}(t) = \sum_k G_{\mathrm{R},k}\,P_\mathrm{I}(t-\tau_k), \tag{12}$$

where $G_{\mathrm{R},k}$ is the power gain of mirror source k at distance d_k and delay $\tau_k = \frac{d_k}{c}$. In the following we aim at approximating the sum in (12) by an integration over τ. The gain of a mirror source is approximately equal to

$$G_{\mathrm{R},k} \approx A_\mathrm{R}\;\underbrace{\frac{1}{4\,\pi\,d_k^2}}_{\text{Free space loss}}\underbrace{(1-\bar{a})^{\bar{w}\,\tau_k}}_{\text{Wall reflection}}, \tag{13}$$

$$= \frac{A_\mathrm{R}}{4\,\pi\,(c\,\tau_k)^2}\,\exp(\bar{w}\,\tau_k\,\ln(1-\bar{a})),$$

where $\bar{w}$ is the average number of wall interactions per second, which can be further approximated as $\bar{w} \approx \frac{c\,S}{4\,V}$ [11]. The number $N(\tau)$ of mirror sources with delay $\tau_k < \tau$ is approximated as the ratio of the volume of a sphere of radius $c\tau$ by the room volume:

$$N(\tau) \approx \frac{4\pi\,c^3\tau^3}{3\,V}\,u(t-\tfrac{d}{c}). \tag{14}$$

The rate of arrival of the signals originating from the mirror sources is obtained by differentiating (14) with respect to τ as

$$r(\tau) \approx 4\pi\frac{c^3\tau^2}{V}\,u(t-\tfrac{d}{c}). \tag{15}$$

With this rate the sum in (12) is approximated by the integral

$$P_\mathrm{R}(t) = \int_{-\infty}^{\infty} P_\mathrm{I}(t-\tau)\underbrace{c\,A_\mathrm{R}\frac{1}{V}\exp\left(-\frac{\tau}{T_\mathrm{Eyr}}\right)u(\tau-\tfrac{d}{c})}_{G_\mathrm{rev,Eyr}(d,\tau)}\,\mathrm{d}\tau. \tag{16}$$

From this expression we conclude that reverberation time T_Eyr is

$$T_\mathrm{Eyr} = -\frac{4\,V}{c\,S\,\ln(1-\bar{a})}. \tag{17}$$

C. Remarks

The parameters of Sabine's and Eyring's models can be summarized as follows:

$$G_{0,\mathrm{rev}} = c\,A_\mathrm{R}\frac{1}{V}, \tag{18}$$

and the decay rates (10) and (17) expressed for both models in the form

$$T = f(\bar{a})\frac{4\,V}{c\,S}, \tag{19}$$

which differ only in $f(\bar{a})$:

$$f(\bar{a}) = \begin{cases} f_\mathrm{Sab}(\bar{a}) = 1/\bar{a}, & \text{Sabine} \\ f_\mathrm{Eyr}(\bar{a}) = -1/\ln(1-\bar{a}), & \text{Eyring.} \end{cases} \tag{20}$$

Consequently, the reverberation times of distinct rooms with the same coefficient $f(\bar{a})$ only depend on their respective volume-surface ratios with unit [m]. It was shown in [5] that $f_\mathrm{Sab}(\bar{a})$ can be interpreted as a first order Tailor series expansion of $f_\mathrm{Eyr}(\bar{a})$ and that this approximation is appropriate for rooms with small absorption coefficients. The decay rates and the exponential decays of Sabine's and Eyring's models are depicted versus $\bar{a}$ in Fig. 2 and in Fig. 3 respectively for comparison purpose. Fig. 2 shows that (10) and (17) rapidly decay in the range of "small" values of $\bar{a}$, i.e. $\bar{a} \lesssim 0.3$, and flatten in the range of "large" values of $\bar{a}$, i.e. $\bar{a} \gtrsim 0.3$. These distinct behaviors may be of importance for experimental investigations of the reverberation time in room electromagnetics, where typical experimentally observed absorption coefficients are larger than those prevailing in room acoustics. Therefore, we expect only small changes of the electromagnetic reverberation time when varying the absorption coefficient of a room.

The absorption coefficient $\bar{a}$ can be obtained from an estimate of the reverberation time $\widehat{T}$ by solving (10) and (17) with T replaced by this estimate:

$$\widehat{a}_\mathrm{Sab} = \frac{4\,V}{c\,S\,\widehat{T}}, \tag{21}$$

$$\widehat{a}_\mathrm{Eyr} = 1 - \exp\left(\frac{-4\,V}{c\,S\,\widehat{T}}\right). \tag{22}$$
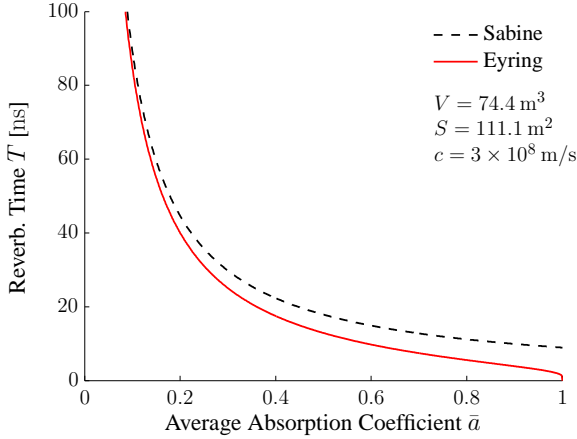
Fig. 2. Graphs of the reverberation times of Sabine's and Eyring's models ((10) and (17)) versus the average absorption coefficient. We selected c as the speed of light.
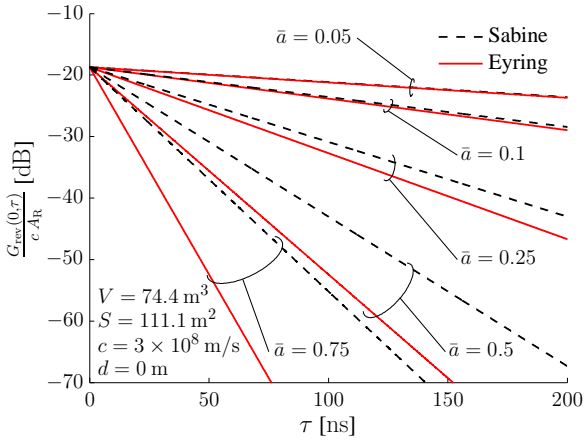

Fig. 3. Graphs of a scaled version of the reverberant component $G_{\mathrm{rev}}(0, \tau)$ with Sabine's and Eyring's decay rates ((10) and (17) respectively) for various values of the average absorption coefficient.

Fig. 4. Investigated environment: (a) schematic floor plan with the selected positions of the receiver (Rp1, ..., Rp9) and the tracks (T1, ..., T3) along which the transmitter was moving; (b) photo of room R4 seen from the position Rp4 with the windows open according to Configuration E; (c) panograph ($360° \times 180°$) of room R3 at receiver position Rp6.

Since $\bar{a}_{\mathrm{Eyr}} = 1 - \exp(-\bar{a}_{\mathrm{Sab}})$, we can transform the absorption coefficient of one model into the other and vice versa. Using this mapping, we provide in Table IV an overview of observed reverberation times and their corresponding absorption coefficients from open literature.

III. MEASUREMENTS AND POSTPROCESSING

A. Measurements

Special care has been taken in the planning of the measurement campaign in order to allow a validation of the reverberation models, see the discussion in Section IV. The measurement campaign was conducted in the premises shown in Fig. 4 consisting of a meeting room (R4) and two adjacent offices (R3 and R2). The inner walls are made of plaster boards. As visible in Fig. 4b, the outer wall consists mainly of windows (W1–W9) separated by concrete pillars. The windows have metallic frames and their glass is metal coated.

The measurements were performed using the RUSK-DLR channel sounder [17] with the settings specified in Table I. The sounder allows for single-input multiple-output measurements. The transmitter and the receiver are synchronized to a common rubidium clock via cables. The sounder was located and operated outside the rooms where the measurements were performed. Antennas positioned in these rooms were connected to the receiver frontend via cables running through small door gaps. The environment was static and no one was in the rooms during the measurements. An omni-directional antenna with $3\,\mathrm{dBi}$ gain [18] was used at the transmitter. The receiver was equipped with a uniform circular array of diameter $75.18\,\mathrm{mm}$ consisting of eight monopoles. The eight output signals of the array were used in the investigations to average out fast fading.

Nine positions were selected in the investigated rooms where the antenna array of the receiver was placed (Rp1 to Rp9 in Fig. 4a). The transmit antenna was mounted on

TABLE I
SETTINGS OF THE CHANNEL SOUNDER.

Sounder Settings	Value
Carrier frequency f_c	5.2 GHz
Bandwidth B	120 MHz
Number of sub-carriers N_c	1536
Carrier separation Δ_f	78.125 kHz
Signal duration T_S	12.8 µs
Cycle duration T_C	204.8 µs
Cycles per burst C	20
Burst duration T_B	4096 µs
Burst repetition time T_{BR}	131.072 ms
Transmit power	0 dBm
Delay MUX and cable τ_{mux}	3.86 ns
Number of Rx antennas M	8

a model train which could move on three tracks (T1, T2, and T3 in the same figure). The train was operated from outside the investigated rooms. Positions Rp1 to Rp9 and the trajectories along the tracks were measured with a tachymeter. The model train was equipped with an odometer connected to the channel sounder to record the transmit antenna location during the movement. The used receive and transmit antennas are vertically polarized. They were placed at a height of 1.26 m and 1.1 m respectively. The height of the furniture was generally lower than that of the antennas except in R3 where the shelves and a newsstand were higher. However, line of sight prevailed for all in-room measurements.

One or more measurements were carried out with the antenna array of the receiver located at each of the nine selected positions and the transmitter moving along each of the three tracks. For the sake of clarity the measurement(s) performed with receive antenna located at Rp and transmitter moving along track T, as well as the collected data, are labelled with the pair (T, Rp).

During one measurement, frequency responses were recorded while the transmitter was moving along the track with a constant speed of approximately 0.05 m/s corresponding to a displacement of 0.0035λ within a burst[1]. Over this distance the channel response can be considered constant. Between two consecutive bursts, the transmitter moved $\lambda/8.8$. For more details on the description of the measurement campaign we refer to [3]. For the validation step V1 the measurements were conducted with the window configurations (opened/closed) depicted in Table II. Note that opening a window prevented to measure with the transmitter moving along track T2.

B. Postprocessing

We now describe how the measurement data were postprocessed to estimate T and $G_{0,rev}$.

In a first step the delay power spectra were estimated as follows. The measured frequency responses collected in each cycle of a burst were averaged to reduce the influence of noise. We denote by $\widehat{H}_{m,r,p,t}[f]$ the averaged frequency response[2] for

[1]A burst contains measurements of C cycles through all transmit and receive antenna combinations, see Table I for the details on the timing of the switching.

[2]The brackets indicate that the variable given as an argument has been discretized.

receive array element m at receiver position r and at transmitter positions p along track t. Estimates of the delay power spectrum at receiver position r and at transmitter positions p along track t were obtained by averaging $\widehat{H}_{m,r,p,t}[f]$ over the receive antennas:

$$\widehat{G}_{r,p,t}[\tau] = \frac{1}{M} \sum_{m=1}^{M} \left| \text{IDFT}\left\{ \widehat{H}_{m,r,p,t}[f]\, W[f] \right\} \right|^2. \quad (23)$$

Here, IDFT$\{\cdot\}$ is the inverse discrete Fourier transform and $W[f]$ denotes a Hann window applied to suppress sidelobes. Depending on the length of the used track, we obtained between 350 and 460 estimated delay power spectra at each position of the receiver array.

In a second step, a least square regression line was fitted to $\log(\widehat{G}_{r,p,t}[\tau])$. All data points of $\log(\widehat{G}_{r,p,t}[\tau])$ for all (r,p,t) indices with delay coordinates in the interval $[\tau_s, \tau_{max}]$ were used for the regression. The slope and the intercept of the line yielded estimates of T and $G_{0,rev}$ respectively. The delay interval was chosen to minimize the influence of the primary component and noise on the slope estimate. We selected $\tau_s = 25$ns, which is the delay sample closest to the propagation time along the maximum transmitter-receiver distance occurring in the measurements plus one pulse duration. The value $\tau_{max} = 150$ ns was chosen such that the influence of noise on the slope estimate is negligible for all measurements.

For a given distance d, $\widehat{G}[d, \tau]$ denotes the spatial average of $\widehat{G}_{r,p,q}[\tau]$ over all transmitter and receiver positions with distances belonging to a 2-wavelength-long segment centered around d. We obtained $\widehat{G}[\tau]$ as the average of $\widehat{G}_{r,p,q}[\tau]$ over all transmitter positions along the tracks and receiver positions of the respective scenarios, or equivalently as the mean of the estimates $\widehat{G}[d, \tau]$ versus d.

In the following we briefly outline the estimation of the path gain, the mean delay and the rms delay spread. Details are provided in [3]. We estimate the path gain as

$$\widehat{G}_{r,p,t} = \frac{1}{M} \sum_{m=1}^{M} \frac{1}{B} \sum_{i=0}^{N_c-1} |\widehat{H}_{m,r,p,t}[i\Delta_f]|^2 \Delta_f. \quad (24)$$

The mean delay and the rms delay spread are estimated from the restriction of $\widehat{G}_{r,p,q}[\tau]$ to the range where this function takes values (in dB) larger than $\theta = 9$ dB above the noise floor, see Fig. 5. The limited bandwidth of the measurement system affects the estimation of the rms delay spread. We compensate for this by subtracting the second central moment of the inverse Fourier transform of $W[f]$ from the second central moment of the restriction of $\widehat{G}_{r,p,q}[\tau]$.

IV. MODEL VALIDATION

Model validation here means verification of the model prediction ability, i.e. testing that the model predictions are in good agreement with measurement data that were not used in the model fitting process. Model validation requires a careful design of the experiment and a proper evaluation in order to avoid circular reasoning when proposing a model.

First, we review the literature proposing reverberation models in room electromagnetics. Thereafter, we present a general validation procedure and detail it with our experiment.

A. Review of Existing Reverberation Models and their Validation Procedures

Sabine's model has already been transcribed from acoustics to electromagnetics [8], [9], [15]. In these contributions, the model is fitted to measurement data collected in a single room, but it is not validated. The model of the delay power spectrum proposed in [6] partly builds upon Eyring's results [5]. The model considers the transition from a non-reverberant to a reverberant field. It leads to a non-exponentially decaying reverberant component. The model was further extended by Rudd in [7] for asymmetrical rooms, where the mean free path length is different from $c/\bar{w}$. Both models in [6] and [7] were partially validated by using two sets of estimated delay power spectra obtained from measurement data collected in two rooms of different sizes. To predict the shape of the delay power spectrum in these rooms, the average absorption coefficient was calculated from the wall materials. The validation of the model was based on a visual assessment of the similarity of the tails of the predicted and estimated delay power spectra[3]. Due to a normalization and the non-exponentially decaying behavior of the spectra's tail the reverberation reference gain was not accounted for in the validation procedure. Neither [6] nor [7] considers modifying the absorption coefficient in a single room to validate the predicted changes of T. Both contributions also discard the influence of neighboring rooms. This, however, may be critical as radio waves may propagate through walls and be reflected backwards into the room under consideration. No comparison to the simpler models by Sabine and Eyring was considered to justify the proposed modifications in [6] and [7].

B. Validation Procedure

We propose a validation procedure of Sabine's and Eyring's models that uses as a criterion the models' ability to predict the reverberation time and the reverberation reference gain. More specifically, we "modify" the characteristics of the investigated room and verify that predictions of the reverberation time match estimated values. A similar approach proposed in [6], [7] consists in collecting measurement data in different rooms of different sizes. However, the interiors of the rooms most likely differ in the used furniture or the wall materials, and thus the volume-surface ratio and the average wall absorption coefficient may change from one room to another, hindering a comparison. To avoid varying all model parameters at once we consider the following four validation steps.

Validation Step V1) Dependency of the Reverberation Time on the Absorption Coefficient: We validate this dependency by comparing predictions of the reverberation time against estimated values, while changing the average absorption coefficient and the surface area in a controlled manner (in the same room). This is achieved by opening one or more windows in room R4. The considered window configurations are reported in Table II.

[3]We remark that in [7] the model of [6] did not provide a valid result for their measurements. In fact an absorption coefficient of 0.6 instead of 0.3 provided a good fit, this large discrepancy leads the author in [7] to their modifications.

The average absorption coefficient a_{w} for the walls, windows, etc. is obtained from a reference measurement with closed windows (Configuration A in Table II). Following Sabine in [4], we set the absorption coefficient for window openings a_{o} to unity, which corresponds to assuming that power leaving the room via an opening never reenters the room. The average absorption coefficient of the room for a given window configuration is modeled as

$$\bar{a} = \frac{S_{\mathrm{w}} \cdot a_{\mathrm{w}} + S_{\mathrm{o}} \cdot a_{o}}{S_{\mathrm{w}} + S_{\mathrm{o}}} = \frac{S_{\mathrm{w}} \cdot a_{\mathrm{w}} + S_{\mathrm{o}}}{S_{\mathrm{w}} + S_{\mathrm{o}}}, \qquad (25)$$

where S_{o} is the area of the window openings with absorption coefficient a_{o} and S_{w} is the area with absorption coefficient a_{w}. The windows open inwards, which we account for in the calculation of S_{w}. For instance, in Configuration B S_{w} is increased by one window area (former outside area) compared to its value in Configuration A.

We use the measurement from Configuration A (all windows closed) to estimate a_{w}. Then the reverberation times for Configurations B – F can be predicted using the average absorption coefficient, obtained from (25), in Sabine's and Eyring's models.

Validation Step V2) Dependency of the Reverberation Time on the Volume-Surface Ratio: To carry out this validation, we consider a second room (R3) smaller in volume compared to room R4. Room R3 contains more furniture than R4, e.g. shelves, office chairs. However, the total surface of the furniture in both rooms is small compared to the total wall surface. Thus, the two rooms have nearly the same average absorption coefficient (approximately equal to the wall absorption coefficient). This rationale leads to the reasonable hypothesis that R3 and R4 have the same value of $f(\bar{a})$ in (19). We predict the reverberation time in room R3 based on measurement data collected in room R4 as follows. In a first step, we estimate the reverberation time from the delay power spectra measured in room R4 (with closed windows). We then plug this estimate and an estimate of the volume-surface ratio for R4 in (19) to obtain an estimate of $f(\bar{a})$ in this room. In a second step we predict the reverberation time in R3 by inserting said estimate of $f(\bar{a})$ and an estimate of the volume-surface ratio for R3 into (19). This procedure is similarly repeated to predict the reverberation time in R4 based on measurement data collected in R3.

Validation Step V3) Dependency of the Reverberation Reference Gain on the Room Volume: In Sabine's and Eyring's models the reverberation reference gain $G_{0,\mathrm{rev}}$ depends, according to (18), only on the volume of the room and the antenna properties but not on the room absorption coefficient. To confirm this property predicted by the models we estimate $G_{0,\mathrm{rev}}$ from measurement data collected in R4 for the different window configurations reported in Table II. If the model holds true, the estimates of $G_{0,\mathrm{rev}}$ obtained for the different window configurations are expected not to deviate significantly.

We also predict $G_{0,\mathrm{rev}}$ in R3 and R4 from measurement data collected in R4 and R3 respectively. Specifically, we compute an estimate of $G_{0,\mathrm{rev}}$ from the measurement data collected in room R4 (R3) with closed windows and the room's volume to estimate the proportionality constant cA_{R} in (18);

then, inserting this estimate in (18) the reverberation reference gain for R3 (R4) can be predicted from the room's volume. Using an estimate of the ratio of the volumes of R4 and R3 in combination with (18) we predict that $G_{0,\mathrm{rev}}$ in R3 is 1.3 dB larger than in R4.

Validation Step V4) Prediction of Path Gain, Mean Delay and Rms Delay Spread: We can predict distance dependent radio channel characteristics, i.e. path gain, mean delay, and rms delay spread by feeding reverberation parameters from Sabine's and Eyring's model into the delay power spectrum model (2). Validation then amounts to the comparison of these predictions with estimates obtained from measurements. To clearly distinguish in terminology, we *predict* the model parameters of (2) (n, G_0, T and $G_{0,\mathrm{rev}}$) but *forecast* the channel characteristics (path gain, mean delay, and rms delay spread).

We predict T and $G_{0,\mathrm{rev}}$ for room R3 based on measurement data collected in room R4 by performing Validation Steps V2 and V3. We assume n and G_0 to be the same for both rooms, thus estimates of these quantities obtained from measurement data collected in one room are used directly as predictions for the other room. The estimates of n and G_0 are obtained as in [3]. These values are inserted into (2) – (4) to forecast path gain, mean delay, and rms delay spread versus distance for room R3. We assess the prediction capability of the reverberation models by means of the root mean square forecasting errors. We repeat the procedure with the roles of R3 and R4 interchanged.

V. Results and Discussion

A. Estimation of the Delay Power Spectrum

The estimated delay power spectra computed from the measurement data collected when both the transmitter and the receiver are located in room R4, i.e. from the data $(\mathrm{T}i, \mathrm{Rp}j)$, $i = 1, 2$, $j = 1, \ldots, 4$, are depicted in Fig. 5. For comparison the fitted exponentially decaying function $\widehat{G}_{0,\mathrm{rev}} \exp(-\tau/\widehat{T})$ (see (4)) is also reported. A visual inspection shows that in the range $[\tau_\mathrm{s}, \tau_\mathrm{max}]$, $\widehat{G}[\tau]$ is well approximated by an exponential decaying function. For short distances, we clearly observe peaks in $\widehat{G}[d, \tau]$ at delays in the range $\tau < \tau_\mathrm{s}$. These peaks originate from line-of-sight propagation and first-order reflections. They are captured by the primary component in model (2). Furthermore, we observe a good fit between the tail predicted by model (2) and the experimental tails. However, for some distances we observe multiple peaks in $\widehat{G}[d, \tau]$ in the range $[\tau_\mathrm{s}, \tau_\mathrm{max}]$. The delay separation between such two contiguous peaks corresponds roughly to twice the propagation time between the (metallic) whiteboard and the windows in room R4, see Fig. 4a. Thus, it seems plausible that these peaks are caused by strong back and forth reflections on these items, so we coin them whiteboard-window (w-w) peaks. Note that in comparison to Fig. 5, the w-w peaks in $\widehat{G}[\tau]$ can be clearly seen in Fig. 6 of Configurations A to D with measurement data $(\mathrm{T}1, \mathrm{Rp}j)$, $j = 2, \ldots, 4$. In Configurations E and F all windows are open, so that the back and forth reflections
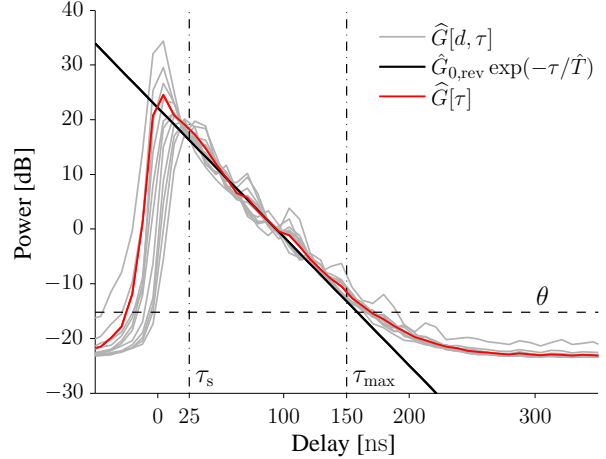

Fig. 5. Spatially averaged delay power spectra $\widehat{G}[\tau]$ and $\widehat{G}[d, \tau]$. For displaying convenience $\widehat{G}[d, \tau]$ is shown for every second distance segment. The reverberation time and reference gain are estimated using the restriction of the estimated delay power spectra to the interval $[\tau_s, \tau_\mathrm{max}]$ indicated with the dash-dot lines. The solid straight line depicts the fitted exponentially decaying function $\widehat{G}_{0,\mathrm{rev}} \exp(-\tau/\widehat{T})$. The dashed line at level θ indicates the threshold for the estimation of mean delay and rms delay spread.

TABLE II
ESTIMATED AND PREDICTED MODEL PARAMETERS FOR WINDOW
CONFIGURATIONS A TO F.

Window Configuration		Meas. Est.		Fit	
Pictograph	$S\,[\mathrm{m}^2]$	$\widehat{G}_{0,\mathrm{rev}}\,[\mathrm{dB}]$	$\widehat{T}\,[\mathrm{ns}]$	$\widehat{a}_\mathrm{Sab}$	$\widehat{a}_\mathrm{Eyr}$
A [W9 R2 | W7 R3 | W5 W4 | W1 R4]	111.1	22.89	18.95	0.47	0.38

Window Configuration		Meas. Est.		Prediction	
Pictograph	$S_\mathrm{w}[\mathrm{m}^2]$ $S_\mathrm{o}[\mathrm{m}^2]$	$\widehat{G}_{0,\mathrm{rev}}[\mathrm{dB}]$	$\widehat{T}[\mathrm{ns}]$	$T_\mathrm{Sab}[\mathrm{ns}]$	$T_\mathrm{Eyr}[\mathrm{ns}]$
B† [R4]	112.68 1.58	22.92	18.07	18.14	17.9
C† [R4]	111.1 3.16	22.87	17.37	17.87	17.4
D† [R4]	112.68 4.74	22.72	16.4	17.15	16.49
E† [R4]	111.1 6.32	22.35	15.74	16.91	16.04
F‡ [R2 R3]	111.1 6.32	22.22	15.8	16.91	16.04

† windows in R2 and R3 closed; ‡ windows in R4 open as in Configuration E

between the whiteboard and the windows (w-w peaks) cannot occur. The presence of the w-w peaks possibly influences the estimates of T. Note that the orientation of the track in room R3 allows for spatial averaging of $\widehat{G}_{r,p,q}[\tau]$, which results in a reduction of the w-w peaks observed in the delay power spectra estimated in this room.

B. Validation Step V1 - Dependency of the Reverberation Time on the Average Absorption Coefficient

One open issue is to determine the relevant surface area to be considered in Sabine's and Eyring's models. Indeed due to wall penetration it is a priori not clear whether the relevant surface area is determined only by the room in
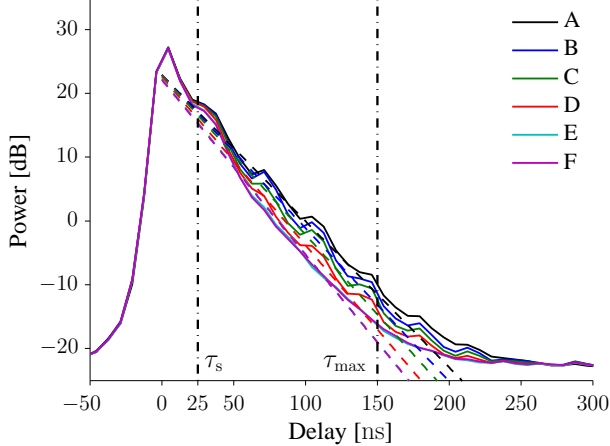
Fig. 6. The delay power spectra $\widehat{G}[\tau]$, obtained as the average of $\widehat{G}_{r,p,q}[\tau]$ over receiver positions Rp2 to Rp4 and all transmitter positions along track T1, are shown for the different window configurations described in Table II. A change of slope, steeper for configurations with more open windows, is visible. The dashed lines correspond to $G_{\mathrm{rev}}(d,\tau)$ with d equal to zero. The dash-dot lines mark the delay interval considered for estimating the reverberation time and the reference gain, which parameterize $G_{\mathrm{rev}}(0,\tau)$. We remark that the estimated delay power spectra in Configurations E and F coincide.

which the transmitter and the receiver are located or if the surface of neighbor rooms needs to be accounted for as well. As can be seen from the results[4] in Table II, Fig. 6 and Fig. 7, opening the windows, i.e. changing the average absorption coefficient, in the neighbor rooms, did not lead to any change in the reverberation time, while in contrast opening windows in the same room did. This indicates that reverberation is confined in the room where the transmitter and receiver are located. It appears from Table II and Fig. 7 that Sabine's model generally predicts too large reverberation times and the prediction error increases when the average absorption coefficient increases. These observations are in line with the theoretical results shown for instance in Fig. 2 and Fig. 3, as well as similar theoretical and experimental results reported in acoustics [5]. The predictions obtained with Eyring's model shown in Fig. 7 are close to the experimental results and their respective confidence intervals overlap except in Configuration E. An explanation for the lower value of T observed in Configuration E and F may be the absence of the w-w peaks in the measured delay power spectra.

In conclusion, this experimental validation confirms that when the receiver and the transmitter are located in the same room, the reverberation is confined in this room and Sabine's and Eyring's reverberation models predict well the relation between the reverberation time and the average absorption coefficient. Eyring's model tends to predict more accurately than Sabine's. Though these results were obtained from exper-

[4]For the results in V1 we use the measurement data (T1, Rpj), $j = 2, \ldots, 4$. The remaining validation steps use the measurement data (Ti, Rpj), $i = 1, 2$, $j = 1, \ldots, 4$ for R4 and (T3, Rpj), $j = 6, 7$.
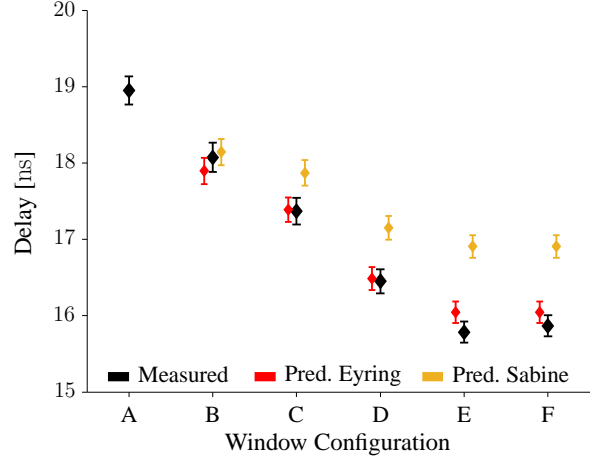

Fig. 7. Estimated and predicted reverberation times. The predictions computed with Eyring's and Sabine's models for (window) Configurations B to F (see Table II) are shown with the 95% confidence interval computed using the reverberation time estimate obtained when all windows are closed (Configuration A).

TABLE III
ESTIMATED AND PREDICTED MODEL PARAMETERS FOR ROOM R4 AND R3. PREDICTIONS FOR ROOM R4(R3) ARE BASED ON PARAMETER ESTIMATES OBTAINED IN R3(R4) AND THE GEOMETRY CHANGES IN R4(R3).

Room	S [m^2]	V [m^3]		G_0 [dB]	n	$G_{0,\mathrm{rev}}$ [dB]	T [ns]
R4	111.1	74.4	est.	-51	1.9	22.3	18.4
			pred.	-52.4	2.3	21.5	18
R3	90.1	55.3	est.	-52.4	2.3	22.8	16.5
			pred.	-51	1.9	23.5	16.9

Note that the predictions of G_0 and n are equal to the estimated values of the other room.

imental investigations carried out in two rooms only, we are confident that they can be generalized to other rooms because i) the considered rooms are "typical" for office buildings and ii) the observed average absorption coefficients are similar to values reported in open literature, see the discussion in Section V-F.

C. Validation Step V2 - Dependency of the Reverberation Time on the Volume-Surface Ratio

Following the procedure described in Section IV-B we plug estimates of the surface, volume and reverberation time for room R4 in (19) to obtain an estimate of $f(\bar{a})$ for this room. By plugging this estimate in (19) with V and S being free variables we obtain a prediction model (line) for the reverberation time that can be applied to any room with a $f(\bar{a})$ value close to that of R4, given the room volume and surface. The prediction line is depicted in black in Fig. 8. The black diamond depicts the point obtained using the estimates of the surface, volume and reverberation time for room R4. From the above procedure this point together with $(0, 0)$ are the anchor points that determine the prediction line. The value of the line at the scaled volume-surface ratio (more specifically an estimate of it) of R3 gives the predicted reverberation time for this room (the grey square in the inset figure in
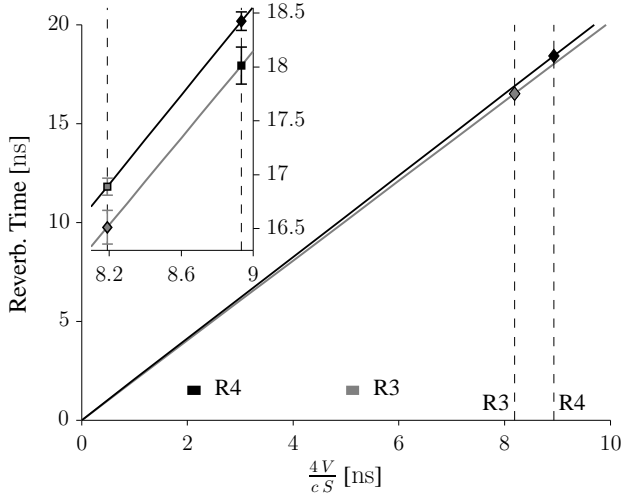
Fig. 8. Reverberation time versus scaled volume-surface ratio. The diamonds indicate the estimates obtained from the data collected in room R3 and R4. The solid lines are prediction curves obtained using model (19) under the hypothesis that $f(\bar{a})$ is equal to the estimate of either room R3 or R4[5]. Predicted reverberation times for R3 and R4 are marked with squares. The zoomed inset figure shows the 95% confidence intervals of the estimates and the predictions.

Fig. 8): $16.9\,\mathrm{ns}$. This value is 2.25% larger than the estimate obtained from measurement data collected in R3 (see the gray diamond in Fig. 8). To cross-validate this result, we repeat the above procedure with the role of R3 and R4 interchanged. The resulting prediction line is depicted in gray in Fig. 8. The difference between the predicted and estimated values of the reverberation time of R4 is 2.3%.

Under the hypothesis that $f(\bar{a})$ is the same for both rooms, the two solid lines are on top of each other. The observed slight deviation between the two prediction lines is the result of a combination of the disparity between the values of $f(\bar{a})$ and errors in the estimation of the room volumes and surfaces. However this deviation is tiny over the considered range of the volume-surface ratio[6].

In conclusion, the above findings confirm the dependency of the reverberation time on the volume-surface ratio as given by (19). To make use of this model, it suffices to tabulate typical values of the average absorption coefficient $\bar{a}$ or of $f(\bar{a})$ for a variety of rooms.

---

[5]For the closed room R4 we observed slightly different estimates for the reverberation time obtained from the data $(\mathrm{T}1, \mathrm{R}pi)$, $i = 2, \ldots, 4$, compared to the values computed from the data $(\mathrm{T}i, \mathrm{R}pj)$, $i = 1, 2$, $j = 1, \ldots, 4$. We conjecture that this is due to the w-w peaks, which are not smoothed by means of spatial averaging when pre-processing the data collected when the transmitter was moving along $(\mathrm{T}1)$.

[6]We remark that the scaled volume-surface ratio of typical office rooms are in the range shown in Fig. 8. This holds true for the rooms reported in Table IV, but the large rooms with a ratio between 20 and 40. For the latter rooms the disparity between the prediction models results in larger errors.

D. Validation Step V3 - Dependency of the Reverberation Reference Gain on the Volume

We first investigate the property predicted by Sabine's and Eyring's models that the reverberation reference gain $G_{0,\mathrm{rev}}$ is unaffected by the average absorption coefficient. To do so we modify the average absorption coefficient in Room R4 by opening the windows in this room and in the neighbor rooms (R2 and R3) according to Configurations A to F, see Table II. Estimates of $G_{0,\mathrm{rev}}$ corresponding to these configurations are reported in Table II. The estimates of $G_{0,\mathrm{rev}}$ corresponding to Configurations B to F only slightly deviate from the estimate obtained for Configuration A (all windows closed). The 95 % confidence intervals of the estimates corresponding to Configurations A to D overlap. The estimates obtained in Configurations E and F deviate from the estimate for Configuration A by $0.54\,\mathrm{dB}$ and $0.67\,\mathrm{dB}$, respectively. We identify two possible causes for these notable deviations: one being the absence of w-w peaks when all windows are open; the other being the impact of the used pulse shape on the estimate of $G_{0,\mathrm{rev}}$. We checked the behavior of the reference gain estimator by means of numerical investigations.

We considered a synthetic exponential-decaying delay-power spectrum with a reverberation time set to a value similar to the estimates obtained in our experiments (Table II) and a pulse shape similar to that of the sounder. We convolved the delay-power spectrum with the squared pulse shape to obtain the effective spectrum including the impact of the system bandwidth from which the estimate of the reference gain is computed. The results revealed that the pulse shape creates differences in the $G_{0,\mathrm{rev}}$ estimates an order of magnitude smaller than the observed differences of $0.54\,\mathrm{dB}$ and $0.67\,\mathrm{dB}$. Thus, the effect of the pulse shape is negligible. From this we conclude that the absence of w-w peaks is most likely the cause of the noticeable difference between the $G_{0,\mathrm{rev}}$ estimate obtained in Configuration A and those obtained in Configurations E and F. Because the estimates corresponding to the remaining configurations fluctuate within their confidence intervals, we also conclude that the reverberation reference gain is unaffected by the average absorption coefficient.

In a second step we predict the reverberation reference gain for rooms with different volumes. The predictions together with the estimates of $G_{0,\mathrm{rev}}$ are reported in Table III. The volume of room R3 is 74% of that of R4 thus the predicted gain $G_{0,\mathrm{rev}}$ is $1.3\,\mathrm{dB}$ larger in R3 than in R4. The estimated reference gain in R3 is $0.7\,\mathrm{dB}$ below the predicted value. For R4 the estimate is $0.7\,\mathrm{dB}$ above the prediction. These observations confirm the volume dependency with some inaccuracy. This disparity is similar to the difference between the estimates of $G_{0,\mathrm{rev}}$ for Configurations A to D and the estimates corresponding to Configurations E and F in R4. From this we conclude that i) a more comprehensive validation requires measurements in rooms with larger volume differences and ii) $G_{0,\mathrm{rev}}$ is insensitive to small changes in the volume. The latter conclusion allows us to estimate the volume of a room based on its boundaries only and ignore possible changes caused by furniture when predicting $G_{0,\mathrm{rev}}$.
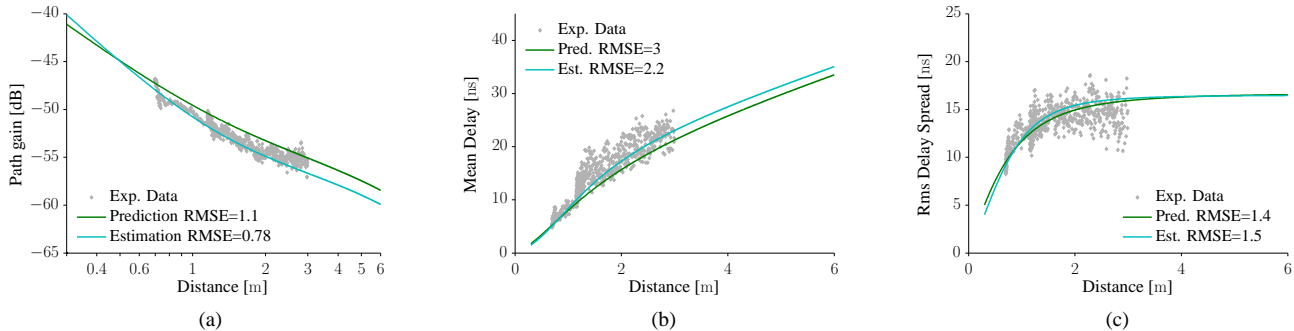
Fig. 9. Path gain (a), mean delay (b) and rms delay spread (c): Experimental values and model forecasts for estimated and predicted parameters of the delay power spectrum model reported in Table III for room R3. The root mean squared error (RMSE) values are presented when the model parameters were estimated from experimental data or predicted with the reverberation models.
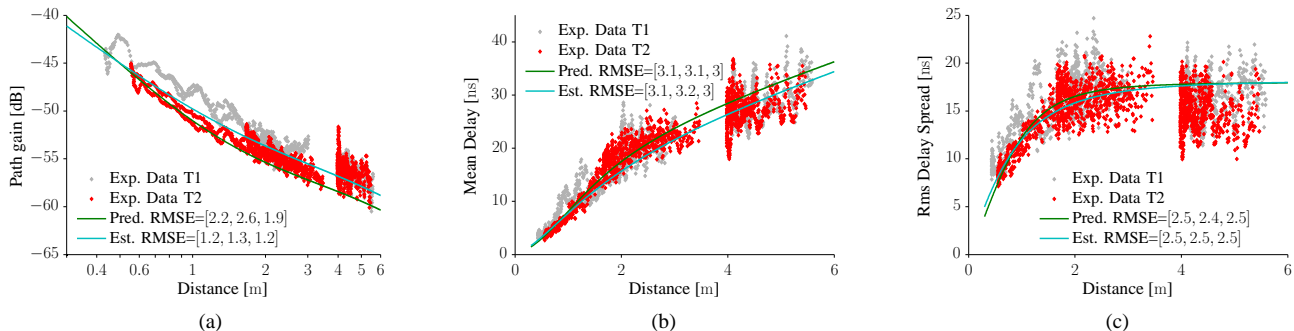

Fig. 10. Path gain (a), mean delay (b) and rms delay spread (c) in Room R4: Estimates computed from measurement data and forecasts obtained from the delay power spectrum model (3) with its parameters set to the estimated and predicted values reported in Table III. The three entries in the reported vectors are the forecast RMSEs computed using the data sets $\bigcup_{i \in I, j=1,\ldots,4}(\mathrm{T}i, \mathrm{Rp}j)$, with $I = \{1, 2\}$, $I = \{1\}$, and $I = \{2\}$.

TABLE IV

OVERVIEW OF VALUES OF THE REVERBERATION TIME AND THE AVERAGE ABSORPTION COEFFICIENT FOUND IN OPEN LITERATURE.

Room Dim. [m³]	V [m³]	S [m²]	Freq. Band [GHz]	$\widehat{\rho}$ [dB/ns]	$\widehat{T}$ [ns]	$\bar{a}_{\mathrm{Sab}}$	$\bar{a}_{\mathrm{Eyr}}$	Comments
$5 \times 5 \times 2.6$	65	102	$1 \ldots 11$	-0.19	22.9	0.37	0.31	Office, read of Fig. 1b NLOS, [19]
$11 \times 20 \times 2.5$	550	595	$5.75 \ldots 5.85$	-0.18	24.1	0.51	0.4	Office, data provided in text, [8]
$7.73 \times 5.85 \times 2.6$	118	161	$2.25 \ldots 2.35$ $2.05 \ldots 2.55$	-0.18 -0.17	24.5 25.8	0.4 0.38	0.33 0.32	Conference room†, [14]
$7.73 \times 5.85 \times 2.6$	118	161	$2.25 \ldots 2.35$ $5.75 \ldots 5.85$	$-0.20 \ldots -0.18$	$22.1 \ldots 24.6$	$0.4 \ldots 0.44$	$0.33 \ldots 0.36$	Conference room‡, [9]
$12 \times 7 \times 2.8$ $3.8 \times 3.5 \times 2.5$	235.2 33.25	274.4 63.1	$2.35 \ldots 2.45$	-0.35 -0.36	12.4 12	0.92 0.59	0.6 0.44	Conference room, read of Fig. 8, [20] Living room, read of Fig. 9, [20]
$4.65 \times 6 \times 3$ $6 \times 9 \times 3$	83.7 162	119.7 198	$59 \ldots 62.5$	-0.58 -0.5	7.5 8.7	1.23 1.26	0.71 0.72	Office, read of Fig. 12a, [21] Office, read of Fig. 12b, [21]
$9.35 \times 7.18 \times 5$	335.7	299.6	$1.25 \ldots 1.75$	-0.2	21.8	0.69	0.5	Laboratory, read of Fig. 13, [6]
$12 \times 53 \times 13$ $10 \times 32 \times 6$ $\varnothing 30 \times 7$	8268 1920 4948	2962 1144 2074	$2.5 \ldots 3$	-0.03 -0.12 -0.08	131 36 56	0.28 0.62 0.57	0.25 0.46 0.43	Big conference room A♭, [22] Big conference room B, [22] Cylindrical conference room C, [22]
$6.6 \times 5.9 \times 3.1$	120.7	155.4	$4.5 \ldots 5.5$ $59.5 \ldots 60.5$	-0.24 -0.5	18.1 8.75	0.57 1.18	0.45 0.69	Conference room ♮, [23]
$5.1 \times 5.25 \times 2.78$	74.4	111.1	$5.15 \ldots 5.25$	-0.24	18.4	0.48	0.38	R4 data $(\mathrm{T}i, \mathrm{Rp}j)$, $i = 1, 2$, $j = 1, \ldots, 4$
$3.79 \times 5.25 \times 2.78$	55.3	90.1		-0.26	16.5	0.5	0.39	R3 data $(\mathrm{T}3, \mathrm{Rp}j)$, $j = 6, 7$

♭ The low absorption coefficient may be caused by metallic air conditioning plates (≈ 45 m²) and the ellipsoidal metallic wire mesh in the ceiling (≈ 636 m²).

♮ The room height in [23] is 3.1 m based on a correspondence with the authors. The reverberation time is the average rms delay spread for NLOS reported in [23] Table IV.

† The value of $\widehat{T}$ is provided in the publication however it is unclear how the values were obtained from the measurements with varying number of people.

‡ A range of median values of $\widehat{T}$ is provided for different polarizations.

E. Validation Step V4 - Prediction of Path Gain, Mean Delay and Rms Delay Spread

Table III reports the estimates and the predictions of the parameters n, G_0, T and $G_{0,\text{rev}}$ of model (2). We use these values to forecast the path gain, mean delay and rms delay spread versus distance. Specifically, we obtain one model forecast by using the parameter estimates and one using the parameter predictions. These models are depicted in Fig. 9 together with the corresponding estimates obtained from the measurement data collected in room R3. We repeat the procedure for R4 in Fig. 10.

We calculate the RMSEs of the model forecasts. The two forecasts yield similar RMSEs for the mean delay and rms delay spread. For the path gain the model forecast using the parameter estimates yields smaller RMSEs than the other. This is expected as the estimates of n and G_0 are obtained from path gain estimates. From these results we draw two conclusions. Firstly, the reverberation models are suitable to predict T and $G_{0,\text{rev}}$ for different environments. Secondly, the delay power spectrum model is well suited to forecast path gain, mean delay and rms delay spread versus distance.

Although the RMSEs obtained with estimated and predicted model parameters are similar, the graphs of the two model forecasts deviate noticeably, see Fig. 9 and Fig. 10. In the following we discuss two possible reasons for this deviation. Firstly, the nature of the primary component observed when the transmit antenna is located on tracks T1, T2, and T3 may differ due to strong first order reflections. This invalidates the assumption that similar values of n and G_0 are observed along all tracks. To illustrate this hypothesis, let's consider the transmit antenna moving on T1 along the metallic whiteboard. Along the entire track, the whiteboard causes a very strong reflection among all other first order reflections that compose the primary component. Possibly, the primary component has higher power compared to those observed along the other tracks, where such a strong reflection does not exist. This difference in powers is visible in the estimated path gains depicted in Fig. 10a, specifically, over short distances ($0.4\,\text{m}$ to $2\,\text{m}$) where the primary component dominates. A more detailed discussion of the difference can be found in [3]. Secondly, the range of distances at which measurements in R3 were taken may be too small to allow for a reliable estimation of n and G_0. Ideally, to obtain good estimates of the model parameters this range of distances should include the transition from a "clearly dominating" primary component to a "clearly dominating" reverberant component. As seen in Fig. 9a for R3, the range only covers the transition phase where both components have almost equal power. Since the estimates of n and G_0 obtained in R3 are used for the prediction in R4, any error in these estimates has an impact on forecasting the channel parameters in R4 and vice-versa.

F. Comparison with Results from the Open Literature

Table IV reports estimates of the reverberation time and the average absorption coefficient computed from the measurement data collected in R3 and R4, as well as experimental values of these parameters gathered from the open literature.

The latter values are either directly available, e.g. explicitly reported in tables, or we have extracted them from depicted experimental delay power spectra. In the latter case, we have obtained the reverberation time estimates manually by reading them from the graphs of the delay power spectra. We did not extract estimates of the reverberation reference gain from these graphs. Indeed, these values cannot be qualitatively compared since the reported delay power spectra are usually normalized in power and/or have been obtained with different measurement set-ups, e.g. equipped with different antennas exhibiting distinct losses.

We observe in Table IV large absorption coefficients at frequencies in the $60\,\text{GHz}$ band [21], [23]. For Sabine's model these coefficients are even greater than unity. If we exclude these values the absorption coefficients computed with Eyring's model fall in the range $[0.25, 0.6]$ with an average of 0.4. In [9] the same reverberation time estimate is reported for the two carrier frequencies $2.3\,\text{GHz}$ and $5.7\,\text{GHz}$. A difference in the estimates of the reference gain is observed, however, it turns out to be close to the expected difference in the antenna losses in these two bands. For the reported rooms in Table IV the reverberation time estimates range from $12\,\text{ns}$ to $25.8\,\text{ns}$. Notice that they are in the range of typically reported values of the rms delay spread [24]. The estimated reverberation times obtained in very large conference rooms range from $36\,\text{ns}$ to $131\,\text{ns}$. Note that a metallic wire mesh hangs from the ceiling and metallic plates from the air conditioning system cover large portions of the walls in the room with a reverberation time of 131ns. We suspect that these items lead to the observed low absorption coefficient and large reverberation time.

In the following we compare our experimental results with those gathered from the open literature, see again Table IV. We observe that the values of the average absorption coefficients obtained for room R3 and R4 are in the range of values found in the open literature. In fact, these values are close to the average value (0.4) of the gathered absorption coefficients in Table IV. It is conjectured in room acoustics that predictions with Sabine's model could be inaccurate when the average absorption coefficient is above $1/3$ and therefore Eyring's model is recommended in this case [25]. This is confirmed by our experimental results showing that Eyring's model provides a better prediction of the parameters of the reverberant component, see Fig. 7 and Table II.

G. Discussion on the Diffuse Field in the Room

Now that Sabine's and Eyring's reverberation models have been validated in in-room environments, it is reasonable to ask whether or not, the tail of the delay power spectrum originates from a diffuse field. Note that our investigations did not address this aspect. In [6], [26] the authors suggest that the tail has an initial build up phase after which the diffuse field occurs. They state that the duration of the build up phase combined with the typical dynamic ranges used in wireless communications does not allow for observing a truly diffuse field. This is especially the case in rooms with large absorption coefficients. Nevertheless, our investigations show that the reverberation models can be applied in in-room radio environments. The fact that Eyring's model was

experimentally shown to predict the change in reverberation time well when the absorption coefficient is altered provide strong evidence supporting this conclusion.

As a matter of fact, the situation is similar in acoustics. It is difficult to show by experiments that the sound field is truly diffuse in real environments [11]. Nevertheless, the reverberation models seem to be applicable in such environments too.

VI. CONCLUSION

Our findings confirm that when the transmitter and the receiver are located in the same room the reverberation is confined in this room and that the reverberation models developed in acoustics can be transposed to electromagnetics in this case. We obtained this result by means of a carefully devised validation procedure with specifically designed experiments which allowed to predict the change of the reverberation time and of the reverberation reference gain when the room properties are altered in a controlled manner. We observed a good agreement between these predictions and experimental results. Specifically, Eyring's model yields more accurate predictions than Sabine's model in rooms with high absorption coefficients. Our estimates of the reverberation time indicate that the average absorption coefficient in the investigated rooms is in the range where Eyring's model is most appropriate.

We used Sabine's and Eyring's reverberation models to predict the values of the parameters of the delay power spectrum model proposed in [3] for an adjacent room. We used these predictions to forecast the path gain, the mean delay and the rms delay spread versus distance in this room. The forecast values of these quantities are in good agreement with experimental results. Thus, the reverberation models can be used to predict the parameters of the delay power spectrum for rooms of different sizes.

The measurement data used for the investigations reported in this contribution were collected in two rooms only, i.e. an office and a meeting room. However experimental values of the absorption coefficient and reverberation time available in the open literature (compiled in Table IV) are similar to our results. We suggest to conduct further measurements in different environments with the purpose to construct a comprehensive environment dependent database of settings for the parameters of Sabine's and Eyring's models.

REFERENCES

[1] H. Hashemi, "The indoor radio propagation channel," *Proc. IEEE*, vol. 81, no. 7, pp. 943–968, Jul. 1993.

[2] Z. Sahinoglu, S. Gezici, and I. Güvenc, *Ultra-wideband Positioning Systems: Theoretical Limits, Ranging Algorithms, and Protocols*. Cambridge University Press, 6 2011.

[3] G. Steinböck, T. Pedersen, B. Fleury, W. Wang, and R. Raulefs, "Distance dependent model for the delay power spectrum of in-room reverberant channels," *IEEE Trans. Antennas Propag.*, vol. 61, no. 8, pp. 4327–4340, Aug. 2013.

[4] W. C. Sabine, *Collected Papers on Acoustics*. Cambridge: Harvard University Press, 1922.

[5] C. F. Eyring, "Reverberation time in "dead" rooms," *J. Acoust. Soc. Am.*, vol. 1, no. 2A, pp. 217–241, Jan. 1930.

[6] C. Holloway, M. Cotton, and P. McKenna, "A model for predicting the power delay profile characteristics inside a room," *IEEE Trans. Veh. Technol.*, vol. 48, no. 4, pp. 1110–1120, 1999.

[7] R. Rudd, "Statistical prediction of indoor radio channel impulse response," Ph.D. dissertation, University of Surrey, Sep. 2007.

[8] J. Andersen, J. Nielsen, G. Pedersen, G. Bauch, and J. Herdin, "Room electromagnetics," *IEEE Antennas Propag. Mag.*, vol. 49, no. 2, pp. 27–33, 2007.

[9] J. Nielsen, J. Andersen, G. Pedersen, and M. Pelosi, "On polarization and frequency dependence of diffuse indoor propagation," in *Vehicular Technology Conference, 2011 IEEE 74th*, Sep. 2011.

[10] D. A. Hill, *Electromagnetic Fields in Cavities: Deterministic and Statistical Theories*, ser. IEEE Press Series on Electromagnetic Wave Theory. Piscataway, NJ: Wiley/IEEE Press, 2009.

[11] H. Kuttruff, *Room Acoustics*, 4th ed. London: Taylor & Francis, 2000.

[12] T. H. Lehman, "A statistical theory of electromagnetic fields in complex cavities," Otto von Guericke University of Magdeburg, Tech. Rep., May 1993.

[13] J. Andersen, K. L. Chee, M. Jacob, G. Pedersen, and T. Kürner, "Reverberation and absorption in an aircraft cabin with the impact of passengers," *IEEE Trans. Antennas Propag.*, vol. 60, no. 5, pp. 2472–2480, May 2012.

[14] A. Bamba, W. Joseph, J. Andersen, E. Tanghe, G. Vermeeren, D. Plets, J. Nielsen, and L. Martens, "Experimental assessment of specific absorption rate using room electromagnetics," *IEEE Trans. Electromagn. Compat.*, vol. 54, no. 4, pp. 747–757, Aug. 2012.

[15] J. B. Andersen, J. O. Nielsen, G. Bauch, and M. Herdin, "The large office environment - measurement and modeling of the wideband radio channel," in *Proc. IEEE 17th Int. Symposium on Personal, Indoor and Mobile Radio Commun. PIMRC 2006*, 2006, pp. 1–5.

[16] R. Valenzuela, "A ray tracing approach to predicting indoor wireless transmission," in *Vehicular Technology Conference, 1993., 43rd IEEE*, 1993, pp. 214–218.

[17] J. Stephan, Y. Lostanlen, J. Keignart, W. Wang, D. Slock, and F. Kaltenberger, "Measurements of location-dependent channel features," ICT- 217033 WHERE, Deliverable 4.1, Oct. 2008, http://www.ict-where.eu/.

[18] Huber+Suhner, "Datasheet for Sencity Antenna For In-Carriage Wireless Communication, Type: SOA 5600/360/3/20/V_1," Document No. 01.02.1358, May 2007.

[19] J. Kunisch and J. Pamp, "Measurement results and modeling aspects for the uwb radio channel," *Ultra Wideband Systems and Technologies, 2002. Digest of Papers. 2002 IEEE Conf. on*, pp. 19–23, 2002.

[20] R. F. Rudd, "The prediction of indoor radio channel impulse response," in *The Second European Conf. on Antennas and Propagation, 2007. EuCAP 2007.*, Nov. 2007, pp. 1–4.

[21] G. Rougeron, F. Gaudaire, Y. Gabillet, and K. Boutouch, "Simulation of the indoor propgation of a 60 GHz electromagnetic wave with a time-dependent radiosity algorithm," *Computers & Graphics*, vol. 26, pp. 125–141, 2002.

[22] F. Heereman, W. Joseph, E. Tanghe, D. Plets, A. Bamba, L. Verloock, and L. Martens, "Performance loss due to multipath propagation for IEEE 802.11 systems," in *Antennas and Propagation (EuCAP), 2013 7th European Conference on*, 2013, pp. 2610–2613.

[23] M. Peter and W. Keusgen, "Analysis and comparison of indoor wideband radio channels at 5 and 60 ghz," in *Antennas and Propagation (EuCAP), 2009. 3rd European Conference on*, 2009, pp. 3830–3834.

[24] M. Awad, K. Wong, and Z. bin Li, "An integrated overview of the open literature's empirical data on the indoor radiowave channel's delay properties," *IEEE Trans. Antennas Propag.*, vol. 56, no. 5, pp. 1451–1468, May 2008.

[25] A. D. Pierce, *Acoustics: An Introduction to Its Physical Principles and Applications*. Acoustical Society of America, Jun. 1989.

[26] C. Holloway, H. Shah, R. Pirkl, K. Remley, D. Hill, and J. Ladbury, "Early time behavior in reverberation chambers and its effect on the relationships between coherence bandwidth, chamber decay time, rms delay spread, and the chamber buildup time," *IEEE Trans. Electromagn. Compat.*, vol. 54, no. 4, pp. 714–725, Aug. 2012.

Gerhard Steinböck received the DI (FH) degree in telecommunications from Technikum Wien, Austria in 1999. From 2000 to 2006, he worked as a R&D engineer at the Austrian Institute of Technology (AIT), Vienna, Austria, contributing among other things in the hard- and software development of a real-time radio channel emulator. Gerhard Steinböck received the M.Sc.E. *(cum laude)* degree in wireless communications in 2008 and the Ph.D. degree in wireless communications in 2013 from Aalborg University, Denmark. Since 2013 he is a postdoctoral researcher at Aalborg University. His research interests lie in the area of wireless communications, radio channel modeling, radio channel estimation and sounding, and radio geolocation techniques.

Wei Wang received his Bachelor degree 2003 in the field of communications engineering from University of Wuhan, P. R. China, Master degree 2006 within the area of digital communications from University of Kiel, Germany, and a doctoral degree 2014 in electrical engineering from University of Erlangen-Nuremberg. Since 2007 he has been employed as a member of the scientific staff at the institute of Communications and Navigation of German Aerospace Center. His research interests are channel characteristics analysis and modeling for localization/navigation based on channel measurements, terrestrial radio based positioning/navigation and related topics.

Troels Pedersen received the M.Sc.E. degree in digital communications and the Ph.D. degree in wireless communications from Aalborg University, Denmark, in 2004 and 2009, respectively. Since 2009 he has been with the Department of Electronic Systems, Aalborg University, first as assistant professor and since 2012 as associate professor. He received the "Teacher of the Year 2011" award by the Study Board for Electronics and IT, Aalborg University. In Spring 2012 he was a visiting professor at IETR, University Rennes 1, France. His research interests lie in the area of statistical signal processing and communication theory, including sensor array signal processing, radio geolocation techniques, radio channel modeling, and radio channel sounding.

Ronald Raulefs is senior researcher and project manager at the Institute of Communications and Navigation of the German Aerospace Center (DLR) in Wessling, Germany. He received the Dr.-Ing. degree from the University of Erlangen-Nuremberg, Germany, in 2008. He has been a visiting researcher at the City University of Hong Kong in September of 2004. He initiated and coordinated the EU FP7 projects WHERE and WHERE2. He holds numerous patents in the area of mobile communications and radio based localization. His current research interests include various aspects of mobile radio communications and localization, such as dynamic resource allocation for cooperative localization.

Bernard H. Fleury (M'97-SM'99) received the Diploma in electrical engineering and in mathematics and the Ph.D. degree in electrical engineering from the Swiss Federal Institute of Technology Zurich (ETHZ), Zurich, Switzerland, in 1978, 1990, and 1990, respectively.

Since 1997, he has been with the Department of Electronic Systems, Aalborg University, Aalborg, Denmark, as a Professor of Communication Theory. He was the Head of the Navigation and Communications Section until 2014. From 2006 to 2009, he was a Key Researcher with the Telecommunications Research Center Vienna (FTW), Vienna, Austria. During 1978-1985 and 1992-1996, he was a Teaching Assistant and a Senior Research Associate, respectively, with the Communication Technology Laboratory, ETHZ. Between 1988 and 1992, he was a Research Assistant with the Statistical Seminar at ETHZ.

Prof. Fleury's research interests cover numerous aspects within communication theory, signal processing, and machine learning, mainly for wireless communications. His current scientific activities include stochastic modeling and estimation of the radio channel, especially for multiple-input–multiple-output (MIMO) systems operating in harsh conditions, iterative message-passing processing with focus on the design of efficient feasible architectures for wireless receivers, localization techniques in wireless terrestrial systems, and radar signal processing. Prof. Fleury has authored and coauthored more than 140 publications in these areas. He is co-inventor on 6 pending and granted patents. He has developed, with his staff, a high-resolution method for the estimation of radio channel parameters that has found a wide application and has inspired similar estimation techniques both in academia and in industry.